Zn-Site Determination in Protein Encapsulated $Zn_xFe_{3-x}O_4$ Nanoparticles

V. L. Pool,[1,2], M. T. Klem,[3,2] J. Holroyd,[1] T. Harris,[3,2] E. Arenholz,[4] M. Young,[5,2] T. Douglas,[3,2] and Y. U. Idzerda[1,2]

[1]*Department of Physics, Montana State University, Bozeman, Montana 59715, USA*
[2]*Center for Bio-inspired Nanomaterials, Montana State University, Bozeman, Montana 59715, USA*
[3]*Department of Chemistry and Biochemistry, Montana State University, Bozeman, Montana 59715, USA*
[4]*Advanced Light Source, LBNL, Berkeley, California 94720, USA*
[5]*Department of Plant Sciences and Pathology, Montana State University, Bozeman, Montana 59715, USA*

(Received September 17, 2008)

The X-ray absorption spectra of the Fe and Zn L-edges for 6.7 nm Fe_3O_4 nanoparticles grown inside 12 nm ferritin protein cages with 10%, 15%, 20% and 33% zinc doping, shows that the Zn is substitutional as Zn^{2+} within the iron oxide host structure. A Neel-Arrhenius plot of the blocking temperature in the frequency dependent ac-susceptibility measurements show that the particles are non-interacting and that the anisotropy energy barrier is reduced with Zn loading. X-ray magnetic circular dichroism (XMCD) of the Fe displays a linear decrease with Zn-doping in sharp contrast to the initial increase present in the bulk system. The most plausible explanation for the moment decrease is that Zn substitutes preferentially into the tetrahedral A-site as a Zn^{2+} cation, generating a mixed spinel.

I. Introduction

There are a number of applications for magnetic nanoparticles: biological detection, magnetic memory devices, cancer treatments, and MRI contrast agents [1-3]. For many applications, it would be beneficial to control the particle moment without size modification. The use of a biomimetic approach, including the synthesis of magnetic nanoparticles inside organic constructs, like protein cages and virus like capsids, both adds additional functionality as well as constraining the encapsulated nanoparticle's volume, resulting in highly monodisperse size distributions [4-9].

The bulk iron oxide Fe_3O_4 is a mixed spinel structure with two structurally inequivalent Fe sites, the A-site (8 Fe^{3+} ions with a 5 μ_B/atom moment) which is tetrahederally bonded to nearby oxygen and the B-site (16 Fe atoms) which is octahedrally bonded. The B-site occupation is further divided into Fe^{3+} valency (8 ions with a 5 μ_B/atom moment) and Fe^{2+} valency (8 ions with a 4 μ_B/atom moment). Indirect exchange coupling through the intervening oxygen atom couples these two sublattices antiferromagnetically to each other resulting in a ferrimagnetic material with a net moment of 1.3 μ_B/atom [10]. Doping Zn into Fe_3O_4 result in Zn^{2+} ions substituting for the tetrahedrally bonded A-site Fe^{3+} ion, initially increasing the net Fe atom moment followed by a subsequent rapid decrease [11]. The crystal $ZnFe_2O_4$ is the terminus (at 33% Zn doping) and is an antiferromagnet with no net moment.

In this study Zn doping has been used as a mechanism to alter the moment of Fe_3O_4 nanoparticles grown in ferritin protein cages. For bulk materials, measuring the magnetization density as a function of Zn concentration was straightforward. For protein-encapsulated nanoparticles, it is extremely difficult to appropriately mass-normalize the magnetization values from typical magnetometry techniques because the mass includes the mass of all the protein cage material (whether they are filled with a magnetic nanoparticle or are unfilled). To circumvent this difficulty, X-ray magnetic circular dichroism measurements are used to establish the variation of the Fe moment with composition.

II. Experimental

For this study 6.7 nm +/-1.1 nm Fe_3O_4 nanoparticles where grown inside ferritin protein cages with and inner diameter of 8 nm and an outer diameter of 12 nm. Details of the synthesis process are provided elsewhere [12]. Dynamic light scattering of the ferritin reaction showed no apparent change in protein diameter. The lack of precipitation and the absence of any change in the exterior diameter of the protein cage suggest that the reaction occurred in a spatially selective manner within the ferritin cage. For this study, Zn doping concentrations of 33%, 20%, 15%, and 10% were used.

X-ray measurements were done at the beamline 4.0.2 and 6.3.1 at the Advanced Light Source (ALS) of the Lawrence Berkeley National Laboratory. Both the X-ray absorption spectroscopy (XAS) and X-ray magnetic circular dichroism (XMCD) spectra of the Fe and Zn $L_{2,3}$-edges were performed at room temperature in the transmission geometry with the nanoparticles dried onto a formvar coated TEM grid. The XMCD spectra were acquired in the presence of a 0.5 T magnetic field with the magnetic field directed along the photon propagation direction using 100% circular polarized light. For

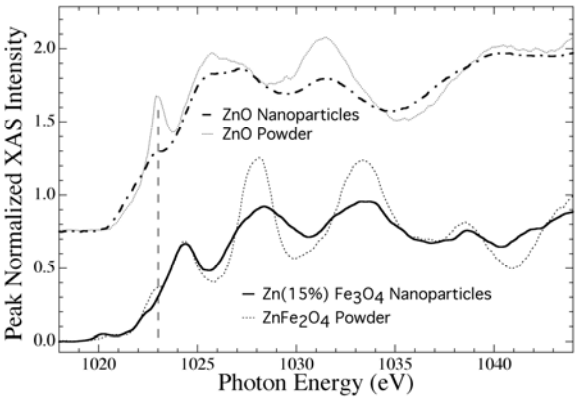

FIG. 1. The XAS of the $L_{2,3}$-edges of 15% Zn-doping of the iron oxide nanoparticles along with a reference $ZnFe_2O_4$ powder and similarly synthesized ZnO nanoparticles and a reference ZnO powder (latter two offset for clarity).

comparison, XAS and XMCD spectra for high purity standards of Fe_3O_4 powders (Aesar), γ-Fe_2O_3 powders (Aesar), ZnO powders (Aesar), $ZnFe_2O_3$ powders (Aesar), and ZnO nanoparticles (similarly synthesized in ferritin protein cages) were also acquired. Vibrating sample magnetometry measurements and temperature dependent ac-magnetic susceptibility (ACMS) measurements were performed at multiple frequencies using the Quantum Design Physical Property Measurement System (PPMS).

III. Results and Discussion

Figure 1 shows the Zn L-edge of 15% Zn in Fe_3O_4 as well as the Zn L-edge for several reference spectra of Zn oxide. (The XAS spectra for the other Zn loading factors that correspond to uniform doping levels of 10%,, 20%, or 33% - the latter corresponding to the $ZnFe_2O_4$ stoichiometry - were identical to the 15% spectra in Figure 1.) It is clear that the Zn is incorporated into the iron oxide nanoparticle rather than forming ZnO clusters within the Fe_3O_4 or as distinct ZnO nanoparticles.

Fe $L_{2,3}$-edge XAS spectra (not shown) for various Zn loading factors are nearly identical to that of Fe_3O_4 and γ-Fe_2O_3 standards. We can conclude that the Zn addition does not dramatically affect the nanoparticle formation and that the Zn is substituting into the tetrahedral A-site as a Zn^{2+} cation.

The small Fe XMCD spectra for these nanoparticles is very similar to the spectra for Fe_3O_4 powders. The Fe L_3-edge XMCD intensity as a function of Zn loading is shown in Figure 2. Also shown is the expected behavior of the nanoparticle net moment for 3 distinct models for Zn substitution and the experimentally determined behavior of the bulk moment. The Fe L_3-edge XMCD intensity displays a linear decline as the Zn concentration is increased.

The simplest explanation of this behavior would be that the Zn is substituting into the octahedral B-site as Zn^{2+} rather then the tetrahedral A-site. The net Fe moment behavior of this scenario is represented by the B-site curve in Figure 2. Though there has been some work to suggest that Zn can substitute into the octahedral B–site in significant amounts in the smaller nanoparticles [13], this seems highly unlikely given the agreement of the Zn XAS spectra with the spectra of tetrahedrally bonded Zn. Also, literature suggests that the octahedral occupation is accomplished under harsh synthesis conditions [14], and the conditions used here are the mildest reported.

The second model represents the initial magnetic behavior of Zn doping that occurs in the bulk. Here, Zn^{2+} substitutes into the Fe^{3+} A-site accompanied by a valence change in a nearby B-site (from Fe^{2+} to Fe^{3+} with a corresponding moment increase from 4 μ_B/atom to 5 μ_B/atom) to retain charge neutrality. The net result is an increase in Fe moment as displayed in the line labeled A-site Case 1 of Figure 2.

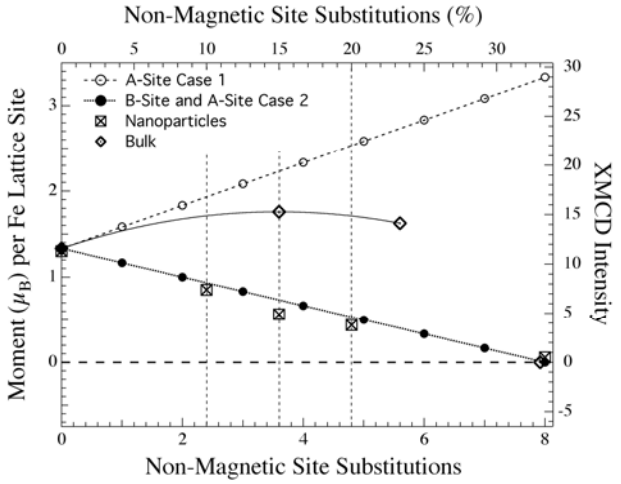

FIG. 2. The XMCD intensity of the L_3-edge of Fe and the extracted moment per Fe lattice site for various concentrations of Zn doped into Fe_3O_4 nanoparticles. Also shown are the experimental bulk values (Ref. 10) and the expected moment for three models described in the text.

The true bulk behavior is more complicated. As described in Morrish [10], as an increasing number of A-sites are occupied by non-magnetic Zn atoms, the A-B antiferromagnetic indirect exchange coupling weakens and a competing indirect exchange coupling within the B-sublattice becomes dominant. As a result, the bulk material shows an initial rise in moment as Zn is substituted, then the moment falls as reported in Figure 2.

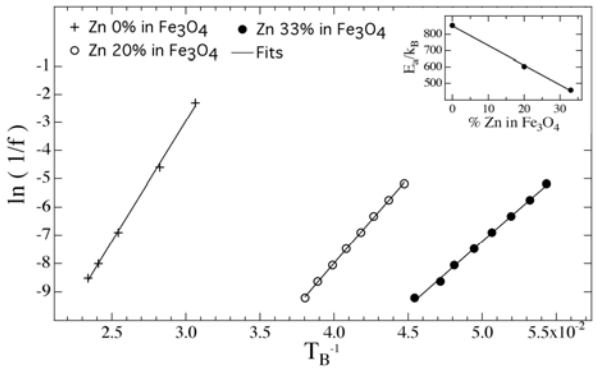

FIG. 3. The frequency dependence of the extracted blocking temperature of the real part of the ac-magnetic susceptibility of the Zn-doped iron oxide nanoparticles for 33%, 20%, and 0%. Inset: The least-squares-fit anisotropy energy vales, reported as E_a/k_b vs. Zn doping.

The third model represents a case where the iron-oxide is in some mixed phase between Fe_3O_4 and γ-Fe_2O_3 due to oxygen deficiencies [15] and that the coupling is distinctly different form in bulk Fe_3O_4. In this case, if the indirect exchange coupling within the B-site were dominant from the outset (with no Zn present), then the linear decline in the moment would correlate perfectly with the increasing Zn concentration in the A-site. The moment would be observed to decrease linearly, labeled A-site Case 2, identical to the behavior for B-site substitution displayed in Figure 2.

All these models assume uniform Zn distribution in the particles, an alternate explanation for the linear decline in the nanoparticle moment is that adding Zn to the synthesis process does not result in Zn-doped Fe_3O_4, but rather structurally homogeneous phases of mixed Fe_3O_4 and $ZnFe_2O_4$ composition. At 33% loading, all the particles are single phase $ZnFe_2O_4$ with zero net moment while at intermediate loading values, the net moment would display a linear decrease with Zn concentration. This alternate is consistent with the observation that the Fe and Zn XAS spectra for all Zn loading concentrations are identical.

To test this possibility, we have compared the magnetic hysteresis curves and the magnetic anisotropy energies as a function of composition. The observed variations of the hysteresis loops rule out a mixture of anti-ferromagnetic $ZnFe_2O_4$ and ferrimagnetic Fe_3O_4 nanoparticles. Such a mixture would display hysteresis loops that were very similar to each other, when normalized to their individual saturation moments. Also, the VSM loops show no exchange bias that would be expected of a two-phase core-shell system between an anti-ferromagnet and a ferrimagnet as is observed in the Co_3O_4-Fe_3O_4 system [16].

Determining the anisotropy energy density behavior with Zn composition may add insight into the resolution of this problem. The Neel-Arrhenius plot for the multi-frequency ACMS for the different Zn loadings is shown in Figure 4. The linear fit demonstrates that the particles are non-interacting and allows for an extraction of the anisotropy energy in the standard way [17,18]. The extracted anisotropy energy verses Zn loading (inset) shows a linear decrease in the anisotropy energy. In the core-shell model, the Zn addition consumes the Fe_3O_4 in the formation of $ZnFe_2O_4$ reducing the ferrimagnet core size.

IV. Summary

The data suggests that the Zn is substituting as Zn^{+2} into the, tetrahedral A site of the spinel structure. Though this is in accordance to what is seen in the bulk material the magnetic behavior is not the same as for the bulk. It seems most likely that the particles are forming a mixed phase of γ-Fe_2O_3 and Fe_3O_4 particles causing the A-B coupling to no longer dominate. To confirm this result and to understand the coupling in more detail further work is needed.

This work is supported by the NSF under grant NIRT-DMR0210915 and through the Office of Naval Research under grant N00014-03-1 0692. The Advanced Light Source is supported by the U.S. Dept. of Energy under Contract No. DE-AC02-05CH11231.

REFERENCES

[1] M. Allen, et al., Magn Reson Med 54 (2005) 807.
[2] A. Jordan, et al., Journal of magnetism and magnetic materials 225 (2001) 118.
[3] C. Barcena, et al., Chem.Commun., Issue 19 (2008) 2224-2226.
[4] T. Douglas, D. P. E. Dickson, S. Betteridge, J. Charnock, C. D. Garner and S. Mann, Science 269 (1995) 54.
[5] S. Mann and G. A. Ozin, Nature 382 (1996) 313.
[6] T. Douglas and M. Young, Nature 393 (1998) 152.
[7] T. Douglas, E. Strable, D. Willits, A. Aitouchen, M. Libera and M. Young, Advanced Materials 14 (2002) 415.
[8] M. Allen, D. Willits, M. Young and T. Douglas, Inorg. Chem. 42 (2003) 6300.
[9] R. A. McMillan, C. D. Paavola, J. Howard, S. L. Chan, N. J. Zaluzec and J. D. Trent, Nat. Mater. 1 (2002) 247.
[10] A.H. Morrish, *The Physical Principles of Magnetism*; IEEE press; New York (2001).
[11] E.W.Gorter Philips Res. Rept. 9,351 (1954).
[12] T. Harris, V. Pool, M. Klem, J. Holroyd, E. Arenholz, Y.U. Idzerda, M. Young, T. Douglas (in preparation).
[13] E.J. Choi, Y. Ahn, K.-C. Song, J. Magn. Magn. Mater. **301**, 171 (2006)
[14] S. Ammer et al., J. Non-crystalline Solids 345&346, 658 (2004).
[15] G.F. Goya, H.R. Rechenberg, M. Chen, and W.B. Yelon, J. Appl. Phys. **87**, 8005 (2000).
[16] M.T. Klem et al., J.A.C.S. 129 (2007) 107-201.
[17] L. Neel, C.R. Hebd. Seances Acad. Sci. 228, 664 (1949); Ann. Geophys.5,99 (1949).
[18] W.F. Brown, Phys. Rev. 130, 1667 (1963).